Developmental Biology 454 (2019) 156–169

Contents lists available at ScienceDirect

Developmental Biology

journal homepage: www.elsevier.com/locate/developmentalbiology

Morphogenesis of the kidney and lung requires branch-tip directed activity of the Adamts18 metalloprotease

Elisabeth A. Rutledge [a], Riana K. Parvez [a], Kieran M. Short [b,d], Ian M. Smyth [b,c,d], Andrew P. McMahon [a,*]

[a] Department of Stem Cell Biology and Regenerative Medicine, Eli and Edythe Broad-CIRM Center for Regenerative Medicine and Stem Cell Research, W.M. Keck School of Medicine of the University of Southern California, CA, 90089, USA
[b] Department of Anatomy and Developmental Biology, Monash University, Clayton, VIC, 3800, Australia
[c] Department of Biochemistry and Molecular Biology, Monash University, Clayton, VIC, 3800, Australia
[d] Biomedicine Discovery Institute, Monash University, Clayton, VIC, 3800, Australia

ARTICLE INFO

Keywords:
Adamts18
Metalloprotease
Branching morphogenesis
Kidney and lung
Collecting duct
Airways

ABSTRACT

Adamts18 encodes a secreted metalloprotease restricted to branch-tip progenitor pools directing the morphogenesis of multiple mammalian organs. *Adamts18* was targeted to explore a potential role in branching morphogenesis. In the kidney, an arborized collecting system develops through extensive branching morphogenesis of an initial epithelial outgrowth of the mesonephric duct, the ureteric bud. *Adamts18* mutants displayed a weakly penetrant phenotype: duplicated ureteric outgrowths forming enlarged, bi-lobed kidneys with an increased nephron endowment. In contrast, *Adamts18* mutants showed a fully penetrant lung phenotype: epithelial growth was markedly reduced and early secondary branching scaled to the reduced length of the primary airways. Furthermore, there was a pronounced delay in the appearance of differentiated cell types in both proximal and distally positions of the developing airways. *Adamts18* is closely related to *Adamts16*. In the kidney but not the lung, broad epithelial Adamts16 expression overlaps Adamts18 in branch tips. However, compound *Adamts16/18* mutants displayed a comparable low penetrance duplicated ureteric phenotype, ruling out a possible role for Adamts16 as a functional modifier of the Adamts18 kidney phenotype. Given the predicted action of secreted Adamts18 metalloprotease, and broad expression of Adamts18 in branching organ systems, these findings suggest distinct requirements for matrix modelling in the morphogenesis of epithelial networks.

1. Introduction

Branching morphogenesis generates the complex tubular epithelial networks that underpin the architecture and function of many metazoan organ systems (Ochoa-Espinosa and Affolter, 2012; Iber and Menshykau, 2013). Two of the best studied branching networks in mammalian organogenesis are the urine transporting collecting duct system of the kidney and the epithelial airways of the lungs (Osathanondh and Potter, 1963; Saxen and Sariola, 1987; Weibel and Gomez, 1962).

Development of the mouse lung begins at embryonic day (E) 9.5 with the evagination of Nkx2.1-expressing epithelial cells from the ventral anterior foregut establishing left and right primordial lung buds (Morrisey and Hogan, 2010). The lung buds elongate and initiate secondary branching establishing the anlagen for each of the five primary lung lobes by E11.5. Continued branching growth over several days generates the extensive epithelial network of the lung airways. In the early phase of lung development, the branching pattern is highly reproducible, employing distinct branching routines to varying extents at different periods and positions (Metzger et al., 2008; Short et al., 2013).

Development of the definitive (metanephric) mouse kidney begins at E10.5 when an outgrowth of the mesonephric duct, the ureteric bud, establishes contact with a population of predetermined metanephric mesenchyme cells (McMahon, 2016). The interactions between these epithelial and mesenchymal cell types drives kidney development. Mesenchyme cells stimulate branching growth of the underlying ureteric epithelium establishing the urine-transporting, collecting duct network of the kidney. In conjunction with branching epithelial growth, there is an expansion of adjacent, branch-tip restricted, mesenchymal progenitor cells and the commitment of distinct nephron and interstitial progenitor types to differentiation programs. Branching growth in the kidney is

* Corresponding author.
E-mail address: amcmahon@med.usc.edu (A.P. McMahon).

https://doi.org/10.1016/j.ydbio.2019.06.012
Received 12 March 2019; Received in revised form 18 June 2019; Accepted 18 June 2019
Available online 23 June 2019

predominantly through bifurcations at branch tips, where a specific branch angle is conserved over the early course of development and increases at later developmental stages (Short et al., 2013).

Multiple studies have highlighted the critical role of receptor tyrosine kinase (RTK) signaling in the morphogenesis of diverse epithelial networks from flies to mammals (Ochoa-Espinosa and Affolter, 2012). In the mouse lung, Fgf10 and its receptor Fgfr2 are the key drivers (Min et al., 1998; Sekine et al., 1999; De Moerlooze et al., 2000). In the kidney, mesenchyme progenitor-derived Gdnf stimulates Ret signaling in ureteric epithelial branch tips. Mutations in Gdnf or Ret results in kidney agenesis (Schuchardt et al., 1994; Pichel et al., 1996; Sánchez et al., 1996). However, more complex mutational analyses indicate Fgf10 and Fgfr2 also play a role in kidney branching (Ohuchi et al., 2000; Zhao et al., 2004), as do a broader range of other RTK receptors and cognate ligands, their relative contributions varying with the stage of kidney development (McMahon, 2016). In addition to RTK action as a driver of branching epithelial outgrowth, the opposing action of other signaling pathways modulates the response to delimit or modulate branching. For example, Bmp4/Bmp type 1 receptors (Alk3 and Alk6) (Miyazaki et al., 2000) and Slit2/Robo2 (Grieshammer et al., 2004; Wainwright et al., 2015) actions prevent secondary outgrowths of the ureteric bud and the formation of duplicated ureters, a relatively common birth defect with unilateral ureteral duplications occurring in 1% of the population (Nation, 1944). In the lung, a Shh/Ptch1 feedback system modulates positional Fgf10 signaling (Chuang et al., 2003). Human genetic analysis of key developmental regulatory genes identified from mouse studies highlights the relevance of branch tip regulatory factors in human organ development (Pal and Reidy, 2017).

In both the lung and kidney, branching morphogenesis is dependent on the maintenance of stem or progenitors cell types in the epithelial branch tips (Morrisey and Hogan, 2010; McMahon, 2016; Costantini and Kopan, 2010). In the kidney, loss of Ret signaling leads to a rapid exit of cells from the branch tips, and a commitment of progenitors to the formation of mature cell types in stalk regions (Chi et al., 2009; Kuure et al., 2010; Riccio et al., 2016). In addition, proliferation rates are highest in this region of the epithelial network (Michael and Davies, 2004). Branching requires a coordinated action of tip cells to form new branch structures and to extend epithelial growth through surrounding cell populations and extracellular matrix. All of this suggests the diverse and complex actions of epithelial branch tips are likely to be underpinned by particularly interesting cell biology.

Recently, we reported on a screen to identify novel genes exhibiting epithelial branch tip-enriched expression in the developing mouse kidney (Rutledge et al., 2017). *Adamts18* was one such gene with branch tip-enriched expression shared by several organs undergoing branch-tip directed morphogenesis including the lung, kidney, and salivary gland (Rutledge et al., 2017). The Adamts family comprises a structurally diverse family of secreted zinc metalloproteinases (Kelwick et al., 2015). A previous mouse study on Adamts18 identified adult defects in the lens, lung, and female reproductive tract (Ataca et al., 2016) though developmental analysis of the etiology of these phenotypes was confined to the eye. Studies on other family members highlight an ancillary domain, which provide substrate specificity to the cleavage, and thrombospondin-1 motifs and spacer regions that facilitate retention of the protease on extracellular matrix components. Varied functions have been ascribed to other Adamts family members in modulating a variety of normal cellular (extracellular matrix turnover, tissue morphogenesis, blood coagulation, and ovulation) and pathological (arthritis, atherosclerosis, cancer, angiogenesis, and wound healing) processes (Stanton et al., 2011; Kumar et al., 2012).

Here, we have explored the action of *Adamts18*, and its close relative *Adamts16*, in branching growth of mammalian organ systems. The data point to distinct roles for Adamts18 in morphogenesis of the mammalian kidney and lung that determines the size, shape, and organization of each organ system.

2. Results

2.1. Adamts18 shows branch tip-restricted expression within the developing mouse kidney and lung epithelium

Adamts18 is expressed within multiple tip epithelial networks of the mouse embryonic kidney, lung, and salivary gland (Rutledge et al., 2017). To analyze Adamts18 expression in more detail, we examined the developing kidney and lung by whole-mount and section *in situ* hybridization (WISH and SISH, respectively) using *in vitro* transcribed digoxygenin-UTP probes and synthetic RNAscope probes (Fig. 1A-**L**). In the kidney, *Adamts18* was initially expressed specifically within the ureteric bud tips on outgrowth and expression was maintained in branch tips throughout the branching process, with a marked downregulation and eventual cessation of expression shortly after birth when branching has terminated (Fig. 1A–E, K, L). In the lung, *Adamts18* was expressed at the distal tips of the developing epithelial airways throughout the period of branching growth (Fig. 1F–J). As in the kidney, expression in the lung terminated with the cessation of branching growth (E18.5; data not shown).

2.2. Adamts18 regulates branching growth in the mammalian lungs

Adamts18's expression within the tip progenitor population of several branching organs (kidney, lung, and salivary gland; Rutledge et al., 2017) is consistent with a general role in branching morphogenesis. To examine the role of *Adamts18*, we obtained mice carrying an *Adamts18* null allele generated by the trans-NIH Knock-Out Mouse Project (KOMP). A deletion removes 3,616bp directly downstream of the ATG site in exon 1, extending to the termination of exon 3 (Fig. 2A). Deleted regions were replaced by an *E. coli* LacZ gene cassette such that a LacZ transcript encoding the β-galactosidase enzyme initiates from the *Adamts18* ATG. Homozygous *Adamts18*−/− mice are adult viable and were recovered at an expected Mendelian frequency in heterozygote mutant intercrosses ($x^2 = 0.01$, $p > 0.95$) (Fig. 2B).

Lungs were collected from *Adamts18* mutants at E12.5, E13.5, and E15.5 and stained with cytokeratin to label the epithelial airways. To directly compare the same developmental stages, E12.5 embryos were somite-matched while at E13.5 and E15.5 embryos were stage-matched by using limb morphology as a staging mechanism. At E12.5, the primary branch network for all five lobes was reduced in *Adamts18*−/− lungs (Fig. 2C–F). In particular, the accessory lobe, which extends from the right lung branch from which it initiates towards the single left lobe, was markedly shorter and curled at E12.5 (Fig. 2E, F), then curved back on itself by E13.5 (Fig. 2G, H). The lungs grew significantly by E15.5 but remained significantly undersized relative to wildtype or heterozygous littermates and the lobes were distinctly misshapen (Fig. 2I, J). As a consequence of the developmental growth deficiency, adult *Adamts18* lungs were dramatically smaller though we did not observe any loss of adult viability under standard vivarium conditions (Fig. 2K, **L**).

To visualize the embryonic lungs in three dimensions and examine in depth the branching pattern, lungs were collected at E12.5 from embryos with a somite range of 49–51 to eliminate stage differences in comparisons within and across litters. Lungs were immunostained with a cytokeratin antibody to specifically label the developing airway epithelium, and specimens were imaged by optical projection tomography (OPT) to generate a three-dimensional reconstruction of each lung. Epithelial branching metrics and patterns were quantified to generate structural parameters for the lungs (Short et al., 2013; Combes et al., 2014; Fig. 3A–F).

Total epithelial length, total epithelial volume, and tip numbers are significantly smaller in *Adamts18*−/− lungs compared to wildtype and heterozygote somite-matched lung samples (Fig. 3M). The fewer tip number indicates that less branching events have occurred at E12.5 in *Adamts18*−/− lungs. The primary branches of each lobe maintain the general branch pattern for the secondary lateral branches. However,

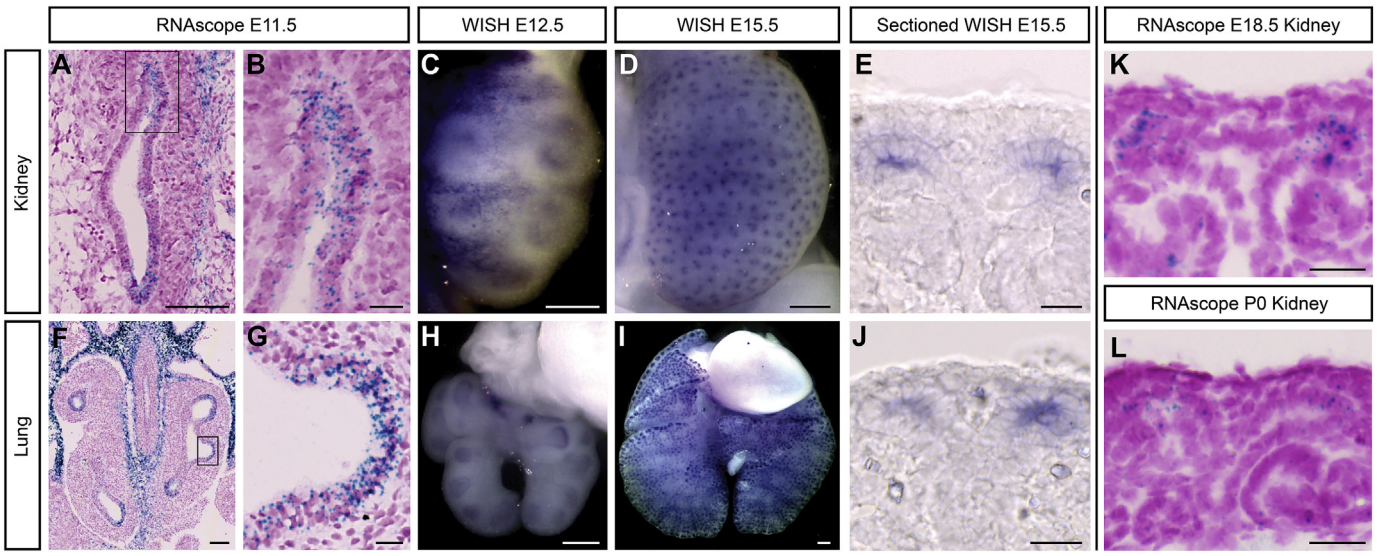

Fig. 1. *Adamts18* is expressed within the tip population in the developing kidney and lung. A-E, K, L: Swiss Webster RNAscope and whole-mount *in situ* hybridization (WISH) of Adamts18 probes in the embryonic kidney. Adamts18 is expressed within the ureteric bud throughout development. By P0 the expression has decreased but still present (L). **F-J**: RNAscope and WISH at various stages of embryonic Swiss Webster lungs with an Adamts18 probe. *Adamts18* is expressed within the lung epithelial tips throughout branching morphogenesis. Boxes in A and F are magnified in B and G, respectively. Line in A, C, F = 100 μm; Line in B, E, G, J, L = 20 μm; Line in D, H, I = 200 μm.

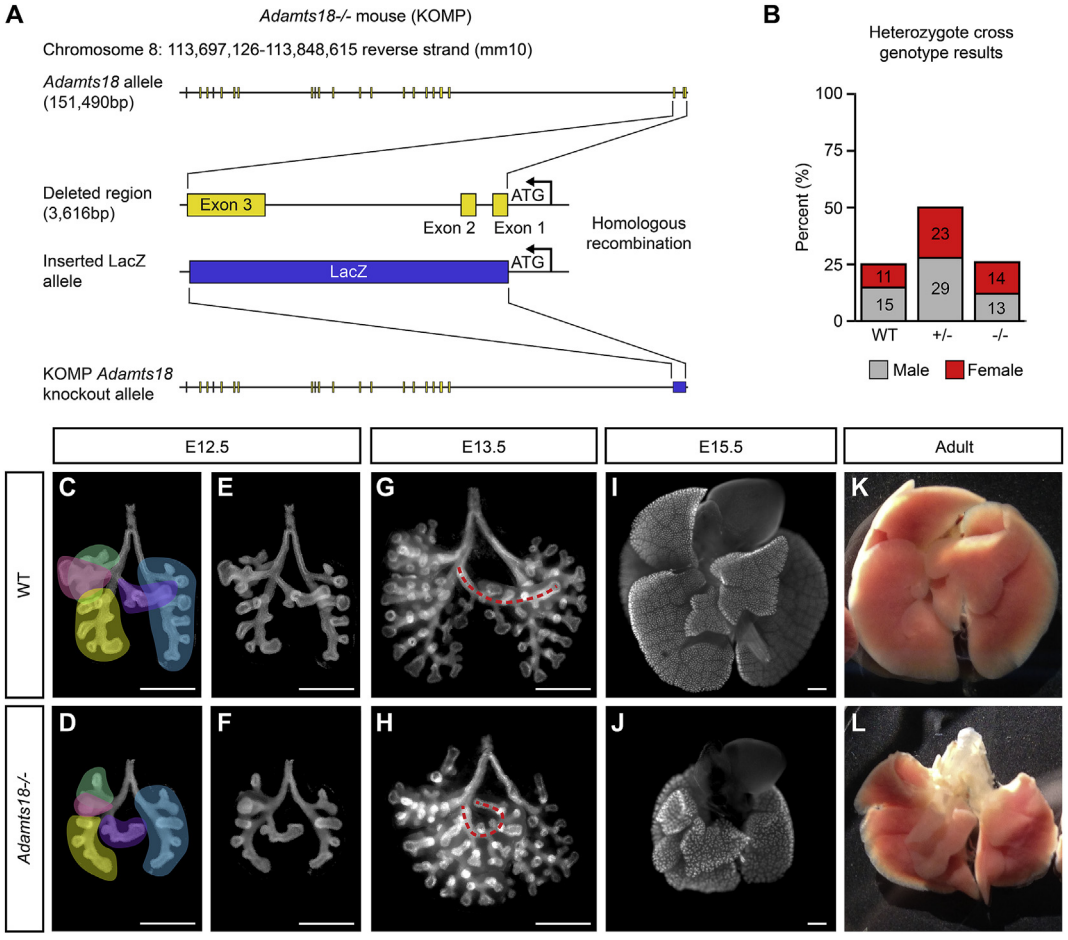

Fig. 2. *Adamts18*−/− lungs are smaller with disoriented branches compared to wildtype counterparts at embryonic and adult stages. A: A schematic of the *Adamts18* knockout mouse acquired from KOMP showing the deleted region and homologous recombination to insert a LacZ sequence in its place (adapted from KOMP's description of the mouse). **B**: The genotyping results of pups born from *Adamts18*+/- crosses demonstrating Mendelian inheritance of the wildtype, *Adamts18*+/−, and *Adamts18*−/− genotypes (numbers on bar graph represent the number counted). **C-J**: Wildtype (C, E, G, I) and *Adamts18*−/− (D, F, H, J) lungs at various stages stained with cytokeratin. The 5 lung lobes are highlighted in C and D: cranial = green, medial = pink, caudal = yellow, accessory = purple, left = blue. **K, L**: Freshly dissected wildtype (K) and *Adamts18*−/− (L) adult lungs. Line = 500 μm.

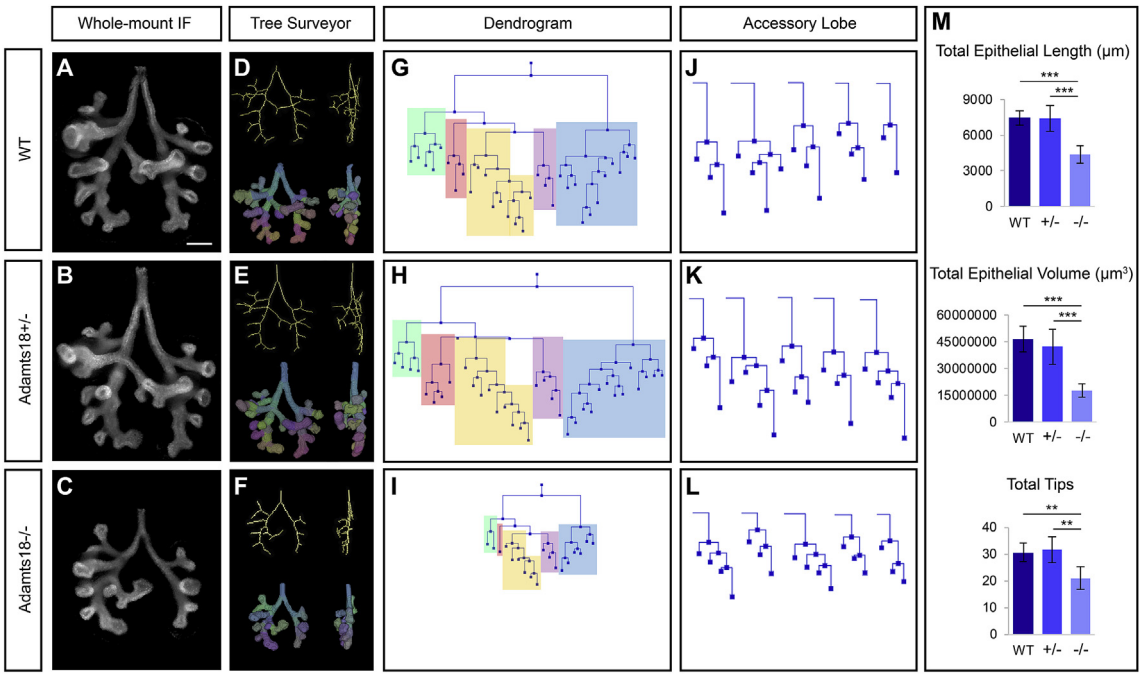

Fig. 3. Optical projection tomography (OPT) and Tree Surveyor analysis of E12.5 *Adamts18*−/− lungs illustrate less epithelium and branch formation compared to stage-matched *Adamts18*+/- and wildtype lungs. A-C: Whole-mount immunostaining of stage-matched Adamts18 E12.5 lungs with cytokeratin were scanned with OPT (n = 5; somite range = 49–51). **D-F:** Three-dimensional skeletal and segmentation models of lungs from A-C generated in Tree Surveyor. **G-I:** Dendrograms displaying the branching pattern for the lungs from A-C. Each lobe is color-coded: cranial = green, medial = pink, caudal = yellow, accessory = purple, left = blue. **J-L:** Dendrograms of each lung's accessory lobe. **M:** Tree Surveyor global analysis quantification. Error bars are SD and significance was determined by a two-tailed *t*-test. ** = $p \leq 0.01$, *** = $p \leq 0.001$. Line = 200 μm.

some branches are absent, suggesting a delay in the initial formation of these secondary branches. For instance, the left lobe within the wildtype and heterozygous lung have five lateral branches present at this developmental stage (Fig. 3A, B). In contrast, the *Adamts18*−/− lung only has three lateral branches (Fig. 3C). To visualize the entire branched network in two dimensions, dendrograms were generated, illustrating the severity of the *Adamts18*−/− phenotype in stage-matched embryos (Fig. 3G–I). The lack of lateral and domain secondary branches in each of the five lobes (indicated by the different colored blocks) in the homozygote lungs is striking. The smaller size of *Adamts18*−/− lungs when compared to wildtype and heterozygous lungs can be attributed to two factors: (1) primary branches are shorter and (2) secondary branching is reduced.

The reduction of primary branch growth and formation of lateral branches is not consistent across all *Adamts18*−/− embryonic lungs. This inconsistency is most likely the determining factor for the variety of misshapen lobes that exist at adult stages. The difference in branch formation is highlighted in the accessory lobe (indicated in purple in Fig. 3G–I), where all individual accessory lobes from each lung quantified are shown (Fig. 3J-L). Although this lobe has generally maintained the number of tips among the genotypes at this stage, the lengths of the branches are shorter in the *Adamts18*−/− compared to *Adamts18*+/- and wildtype (Fig. 3M).

To analyze lobular branching organization, we focused on the left and accessory lobes examining primary branch length and the position of secondary orthogonal branches (Fig. 4A–D). Although *Adamts18*−/− lungs had shorter primary branch lengths than *Adamts18*+/- and wildtype, the segment lengths between lateral secondary branches were proportionally similar across all genotypes for each primary branch of the left lobe, though there was a slight reduction for the accessory lobe (Fig. 4C, D). Thus, despite a reduction in primary branch growth, secondary branching occurs at the expected chronological time point, scaling to the shorter primary branch length for many early branching events. Thus, the primary role of Adamts18 at early stages is in promoting epithelial growth rather than epithelial branching per se. Interestingly, when lungs were examined at E13.5, in addition to an expected decrease in branch and branch tip number in *Adamts18*−/− lungs, we observed an unexpected but significant expansion of lung volumes reflected by increased branch formation in *Adamts18*+/- lungs (Figs. S1A–G). These findings point to a complex relationship between Adamts18 levels and growth programs in the lung.

2.3. The loss of Adamts18 in embryonic lungs delays the expression of specific differentiated cell types

To determine Adamts18's potential molecular role in lung development and differentiation, we performed immunostaining with antibodies recognizing regional and cell type specific epithelial cell markers. No discernable difference was observed in Sox2 (proximal epithelial progenitor cell marker) and Sox9 (distal epithelial progenitor cell marker) distribution examining wildtype and *Adamts18*−/− lungs by whole-mount analysis at E12.5 suggesting that early proximal-distal regionalization of the developing airways is independent of Adamts18 (Fig. 5A–D). Surprisingly, immunostaining to address the distribution of markers of differentiating cell types, Muc5ac (mucosal cell), Sftpc (alveolar epithelial cell type 2), and Tuba4a (ciliated cell), showed no evidence of any of these cell types at E16.5 though the broad epithelial marker Cdh1 was present (Fig. 5E–J). Cdh1 highlights the difference in the epithelial structure between *Adamts18*−/− and wildtype. Quantitative PCR analysis confirmed markedly reduced *Muc5ac*, *Sftpc*, and *Tuba4a* transcripts in the E16.5 *Adamts18* mutant lung (Fig. 5I). Interesting, qPCR analysis at E17.5, demonstrated increased expression of all three genes in Adamts18 mutant lungs (Fig. 5I). By adult stages, the expression of these genes was either comparable to wild type lungs or elevated in *Adamts18*−/− lungs (Fig. 5I). Collectively, the data indicate that the loss of Adamts18 in the lung significantly delays the appearance of specialized cell types arising in both proximal (mucosal and ciliated cells) and distal (alveolar epithelial cells) positions of the developing airways.

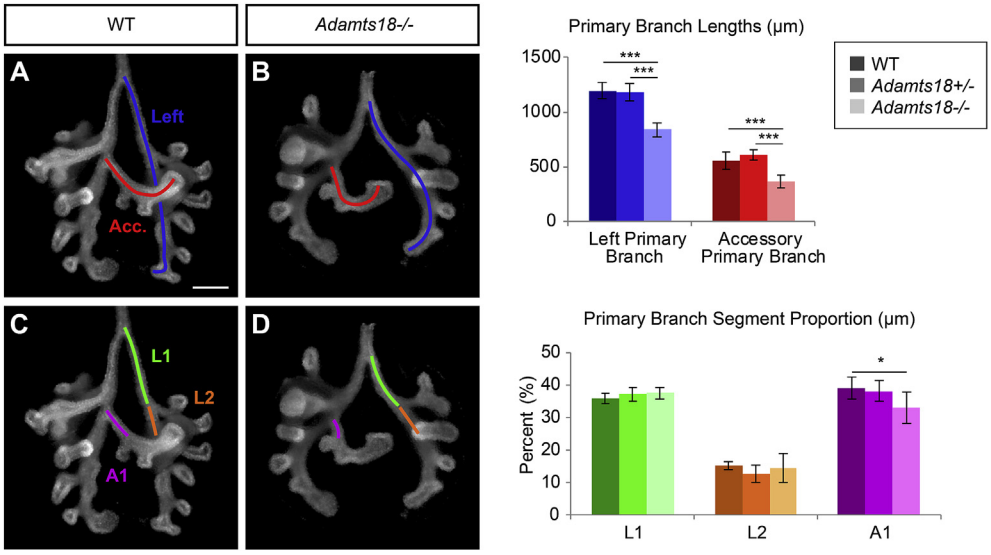

Fig. 4. *Adamts18*−/− have shorter primary branches while maintaining the formation of secondary lateral branches in E12.5 lungs. A, B: The left and accessory (Acc.) primary branch lengths measured on Tree Surveyor are significantly shorter in *Admats18*−/− lungs compared to somite-matched *Adamts18*+/- and wildtype lungs (n = 5, somite range = 49–51). **C, D**: The lengths of the highlighted branch segments (L1, L2, A1) divided by the total length of the primary branch associated with each segment quantifies the primary branch segment proportion. There is no significant difference in segment proportion within the left branch for segments L1 and L2. There is a significant difference between *Adamts18*−/− and wildtype proportion for A1. Error bars are SD and significance was determined by a two-tailed *t*-test. * = p ≤ 0.05, ** = p ≤ 0.01, *** = p ≤ 0.001. Line = 200 μm.

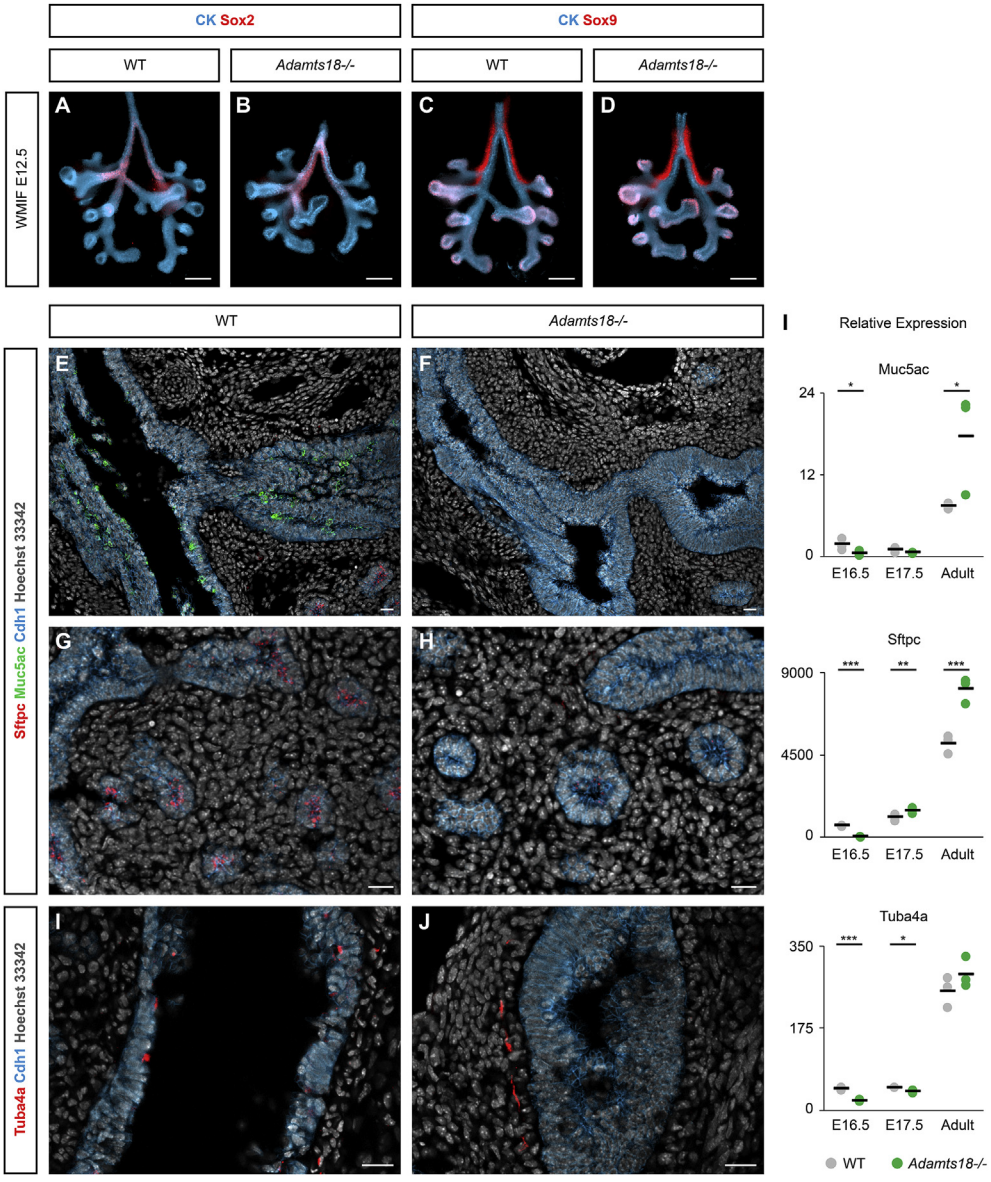

Fig. 5. Progenitor markers showcase similarities while differentiated markers reveal a delay in development between wildtype and *Adamts18*−/− embryonic lungs. A-D: Whole-mount immunostaining with proximal (Sox2) and distal (Sox9) progenitor markers appear similar between wildtype and *Adamts18*−/− E12.5 lungs. **E-J**: Section immunostaining on E16.5 lungs with differentiated cell types, highlighting a lack of mucosal cells (Muc5ac), alveolar epithelial type 2 cells (Sftpc), and ciliated cells (Tuba4a) in *Adamts18*−/− compared to wildtype. **I**: qPCR analysis on *Adamts18*−/− and wildtype lungs at E16.5, E17.5, and adult stages. Black bars are the average between the biological triplicates and significance was determined by a two-tailed *t*-test. * = p ≤ 0.05, ** = p ≤ 0.01, *** = p ≤ 0.001. Line in A-D = 200 μm, line in E-J = 20 μm.

2.4. *Adamts18* regulates ureteric bud outgrowth in the kidney

Next, we examined kidney development in *Adamts18*−/− embryos at E10.5, E11.5, and E12.5 (Fig. 6A–F). At the onset of ureteric bud outgrowth at E10.5, structural irregularities are observed in *Adamts18*−/− (12.5%, 2/16) compared to wildtype (0%, 0/8) (Fig. 6A, B). Emergence of an additional ureteric bud outgrowth can be seen by E11.5 (Fig. 6C, D). Twenty-nine percent of *Adamts18*−/− kidneys (E11.5-E15.5) showed duplicated, unilateral ureteric outgrowths arising from the nephric duct (14/48) and 8% of *Adamts18*−/− kidneys exhibited bilateral duplications (4/48) (Fig. 6K). Unilateral ureteric duplications were observed in wildtype and heterozygous kidneys but at a much lower frequency of 2.2% (1/45) and 3.6% (1/28), respectively. No wildtype or heterozygous embryos collected displayed bilateral double ureters. Of the kidneys with a double ureter, the subsequent branching of the ureteric bud appeared unaffected, suggesting that Adamts18 plays a role restricting outgrowth of the ureteric bud and not in subsequent branching morphogenesis. Interestingly, the duplicated ureteric outgrowth leads to an enlarged kidney at E15.5 that morphologically resembles independently developing fused kidneys (Fig. 6G, H). When nephron numbers were assessed through glomerular counts in adult kidneys (Cullen-McEwen et al., 2012), *Adamts18*−/− kidneys with duplicated ureters showed a significant increase in nephron endowment relative to wildtype, heterozygous mutants, and homozygous mutant kidneys with a single ureter (Fig. 6I, J, L). This suggests that kidney size and the number of nephrons is primarily determined by the number of progenitor niches established by the branching ureteric epithelium and not by the starting number of nephron progenitors at the outset of kidney development.

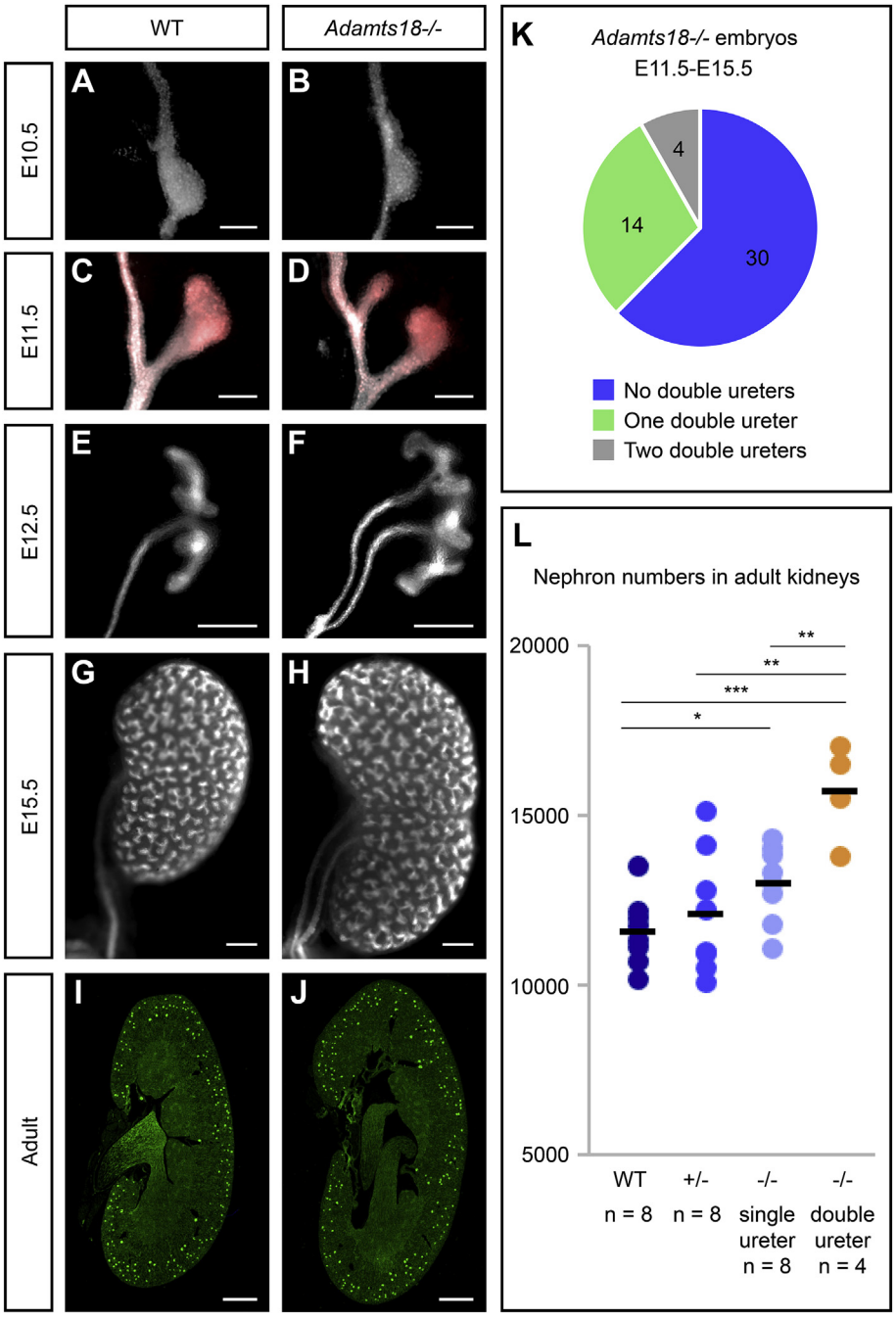

Fig. 6. *Adamts18*−/− kidneys develop double ureters with higher nephron counts. A-H: Whole-mount immunostaining of embryonic kidneys with epithelial marker cytokeratin (white) at E10.5, E11.5, E12.5, and E15.5 illustrating *Adamts18*−/− kidneys with double ureters are larger than wildtype kidneys. C and D are additionally stained with ureteric bud tip marker Ret (red), demonstrating that all outgrowths from the nephric duct express the tip marker. **I, J**: Sections of adult kidneys (6 week) stained with the glomerular marker peanut agglutinin (PNA). **I**: Embryonic *Adamts18*−/− embryos (E11.5-E15.5) have at least one kidney with a double ureter at a 38% frequency. **J**: Adults with double ureters have significantly more nephrons based on PNA staining. Dots represent nephron counts per kidney and the black bar is the average. Error bars are SD and significance was determined by a two-tailed *t*-test. * = $p \leq 0.05$, ** = $p \leq 0.01$, *** = $p \leq 0.001$. Line in A-D = 100 μm; line in E-H = 200 μm, line in I, J = 1000 μm.

2.5. Analysis of the impact of Adamts16 removal on the Adamts18 kidney phenotype

As only one third of *Adamts18−/−* kidneys showed a phenotype, and growth post-branch initiation was not retarded, contrasting a fully penetrant growth retarded lung phenotype, we compared kidneys and lungs for expression of other Adamts18 family members. Of these, *Adamts16* is the most closely related Adamts-family member and has been suggested to play a role in rat testis development (Gopalakrishnan et al., 2012; Abdul-Majeed et al., 2014). However, Adamts16 has not been studied in kidney development.

Adamts16's expression was examined by WISH and SISH analysis of 12.5 and E15.5 wildtype kidneys and lungs. No Adamts16 expression was observed in the developing lung (Fig. 7A, B), but in the kidney, strong expression was observed throughout the ureteric epithelium, including the branch tip and in developing nephron structures (Fig. 7C–F). Thus, a kidney-specific overlap in Adamts16/18 expression domains is consistent with a potential redundancy in the action of these two genes in ureteric branching. To examine this possibility, we used gRNA/Cas9 gene editing to generate a 33bp deletion in exon 1, removing the initiation methionine, generating a likely null allele (Fig. 7G). To determine expression levels of *Adamts16* and *Adamts18* transcripts, qPCR analysis was performed on *Adamts16−/−;Adamts18−/−* and wildtype embryonic kidneys at the site of the engineered deletions (*Adamts18* = exon 3–4; *Adamts16* = exon 1–2) and in transcribed regions downstream of these deletions (*Adamts18* = exon 10–11; *Adamts16* = exon 17–18) (Fig. 7H). As expected, primers examining the deleted regions in *Adamts16* and *18* only detected a transcript in wild-type mRNA. However, mutation of

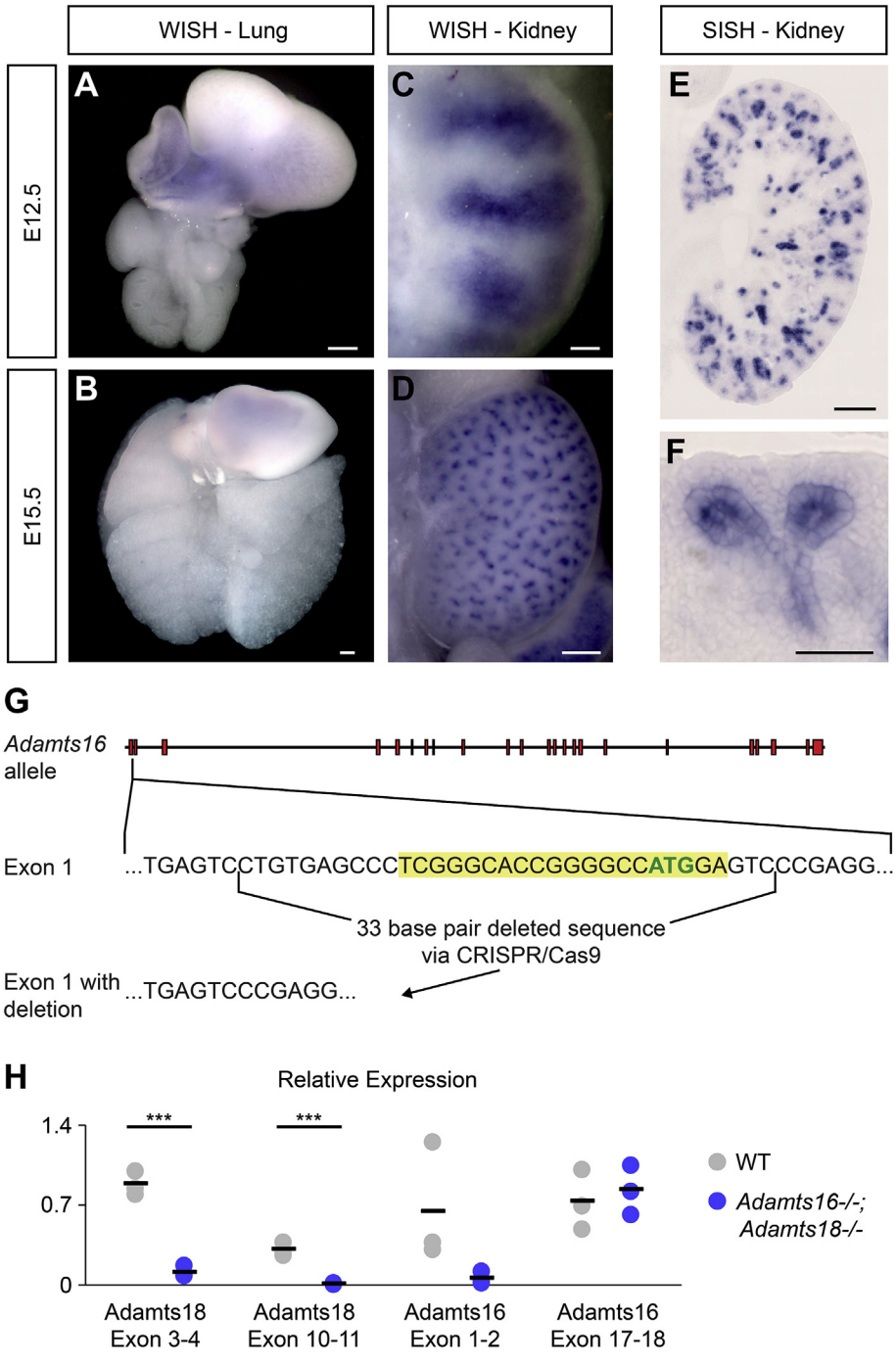

Fig. 7. *Adamts16* is expressed within the ureteric bud and developing nephron structures in the kidney and absent in the lung. A-D: *Adamts16* expression shown in whole-mount *in situ* hybridization (WISH) of Swiss Webster embryonic kidneys and lungs at E12.5 (A, C) and E15.5 (B, D). **E, F**: Section *in situ* hybridization (SISH) of *Adamts16* expression within an E15.5 kidney showing expression in the ureteric epithelium and developing nephron structures. Line in A, B, D, E = 200 μm; Line in C, F = 50 μm. **G**: A schematic of the generation of *Adamts16−/−* mouse utilizing CRISPR/Cas9 technology. The guide RNA sequence is highlighted in yellow, which includes the ATG start site in green within Exon 1 of *Adamts16*. **H**: qPCR analysis for specific regions within the Adamts18 and Adamts16 genes. Black bars are the average between the biological triplicates and significance was determined by a two-tailed *t*-test. *** = $p \leq 0.001$.

Adamts18's but not Adamts16 lead to dramatic reduction in transcription downstream of the deleted region (Fig. 7H). Therefore, although the normal ATG start site was removed in Adamts16 tageting, the remainder of the gene is likely expressed at normal levels, which could result in production of a truncated protein if translation is possible from an in-frame ATG codon downstream of the deletion in the Adamts18 mutant mRNA.

Stage-matched E12.5 (somites = 50–52) kidneys were isolated from single *Adamts18−/−* and double *Adamts16−/−;Adamts18−/−* mutants. Ureteric branching was examined in whole-mount preparations and double ureter formation, branch tip number, epithelial length, and epithelial volume was quantified as in the earlier lung studies (Fig. 8A–J). Loss of *Adamts16* activity did not modify the *Adamts18−/−* phenotype. The frequency of double ureters for *Adamts16−/−;Adamts18−/−* was 35% (17/48) comparable to the 38% observed in *Adamts18−/−* kidneys (15/40) (Fig. 8I). Bilateral double ureter formation, a rarer event, occurred less frequently *in Adamts16−/−;Adamts18−/−* (4%, 2/48) compared with single *Adamts18−/−* mutants (10%, 4/40) (Fig. 8I). Analysis showed that the position of secondary ureter formation varied, but the outcome was similar. Nephrogenic progenitors that normally distribute homogeneously around a single branching network form separate coherent clusters around each of the outgrowths (Fig. 8A–H). While it is difficult to determine whether secondary branching occurs anterior or posterior to the primary outgrowth, we note that anterior and posterior branching networks frequently differ in size with no clear anterior or posterior bias suggesting secondary outgrowth may occur in either position (Fig. 8E–H).

Overall, kidneys with double ureters had significantly more total epithelial length, total epithelial volume, and total tip numbers compared to single ureters regardless of genotype, as expected (Fig. 8J), but no statistical differences were observed in these parameters comparing *Adamts18−/−* and *Adamts16−/−;Adamts18−/−* kidneys with double ureters. Interestingly, regardless of genotype, there was a strong left-right bias in the duplicated ureter phenotype: 70% (7/10) of *Adamts18−/−* and 73% (11/15) of *Adamts16−/−;Adamts18−/−* occurred in the left kidney, which normally adopts a more anterior position in the developing body plan (Fig. S2).

As expected, the loss of Adamts16 within the embryonic lung resulted in no observable phenotype given *Adamts16* is not expressed in this organ (Fig. S3 A, B). Furthermore, *Adamts16−/−;Adamts18−/−* lungs resemble the phenotype of *Adamts18−/−* lungs (Fig. S3 C, D). Thus, the absence of Adamts16 does not contribute to the observed lung phenotype.

2.6. Analysis of cell proliferation and cell death in the Adamts18 epithelial growth phenotypes

Cell proliferation and apoptosis were quantified within the tip populations of both kidneys and lungs at E12.5 (somites = 51–52) by two different time pulses of EdU incorporation (30min and 4hr) and Caspase 3 immunostaining, respectively (Fig. 9A–I). For the lungs, Sox9 co-immunostaining was used to distinguish the distal tips and immediate proximal epithelium (Fig. 9C, D), and β-galactosidase activity from the lacZ allele provided a tip focused reference (Fig. 9A, B). With a 4hr EdU pulse, no reduction in proliferation was observed between epithelial tip cells in *Adamts18−/−* lungs (70% of cells incorporated EdU) compared with stage matched wildtype lungs (65% of cells incorporated EdU).

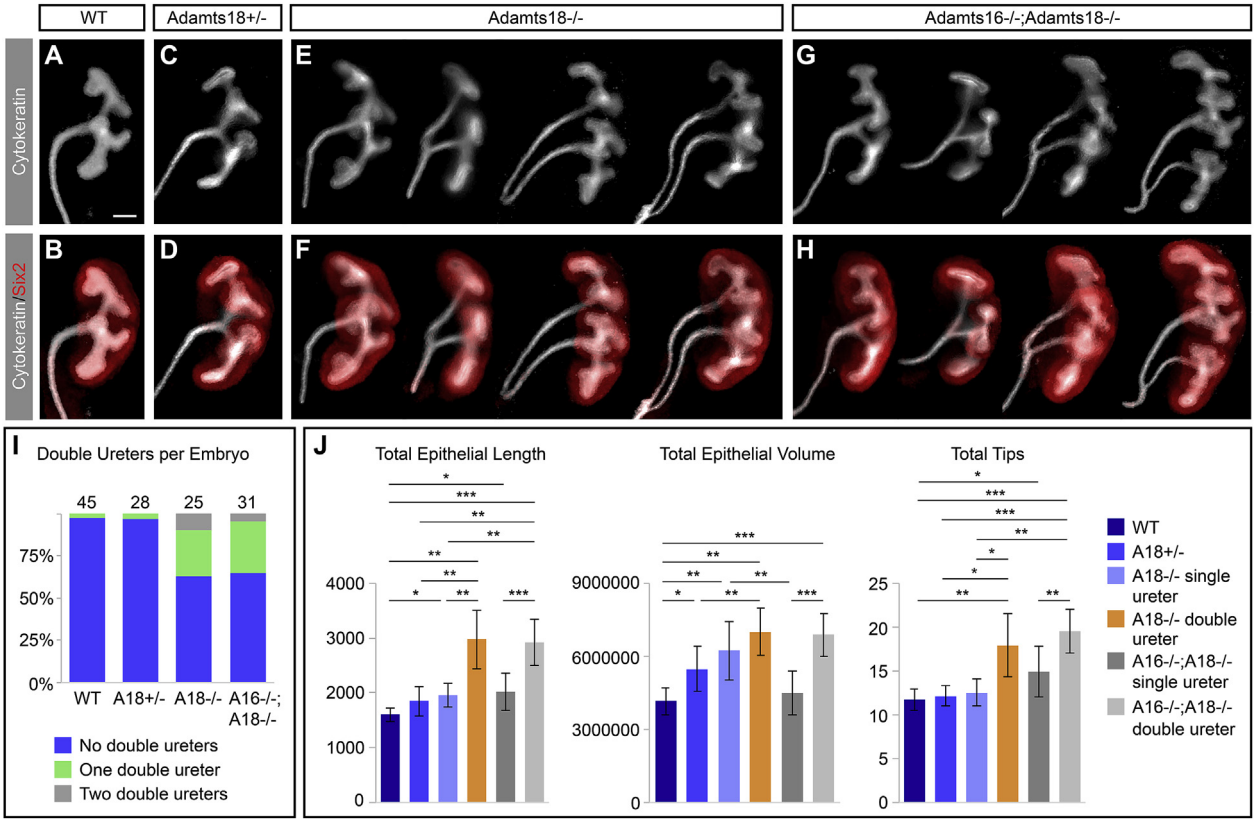

Fig. 8. *Adamts18−/−* and *Adamts16−/−;Adamts18−/−* E12.5 kidneys develop double ureters at similar frequencies. A-H: Whole-mount immunostaining of E12.5 (somite range = 50–52) kidneys stained with cytokeratin (epithelial marker) and Six2 (nephron progenitor marker) demonstrate the structural variation of double ureters observed. **I**: The frequency of double ureters in *Adamts18−/−* (38%) and *Adamts16−/−;Adamts18−/−* (35%) are similar and are significantly higher than the frequency in wildtype (2%) and *Adamts18+/−* (3%). The numbers above the bars are the embryo numbers per genotype. **J**: OPT and Tree Surveyor analysis of the kidneys show that the double ureters for both *Adamts18−/−* and *Adamts16−/−;Adamts18−/−* are higher in total epithelial length, epithelial volume, and number of tips compared to single ureter samples regardless of genotype (n = 5). Error bars are SD and significance was determined by a two-tailed *t*-test. * = $p \leq 0.05$, ** = $p \leq 0.01$, *** = $p \leq 0.001$. Line = 100 μm.

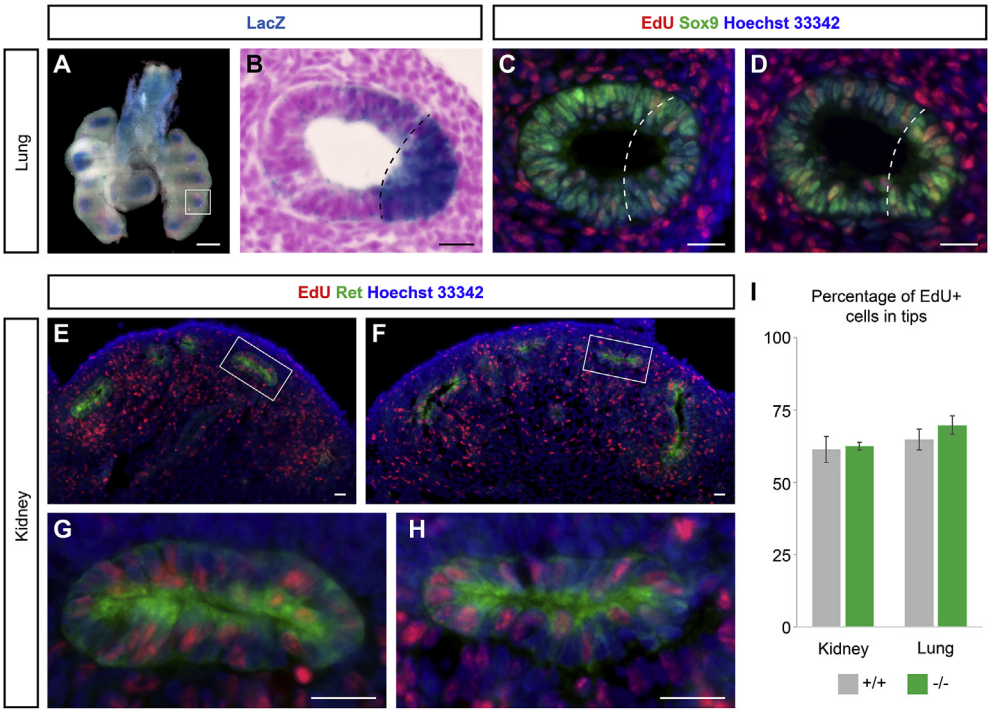

Fig. 9. The percentage of proliferating cells within the tip population of E12.5 kidneys and lungs are consistent between wildtype and *Adamts18*−/− organs. A: Whole-mount LacZ staining of *Adamts18*−/− E12.5 lungs showing tip expression of *Adamts18*. **B**: LacZ section of *Adamts18*−/− of an individual tip with a dashed line highlighting distribution of *Adamts18* expression within the epithelium. **C, D**: *Adamts18*+/+ (C) and *Adamts18*−/− (D) cryosections of lungs immunostained with Sox9, EdU, and Hoechst 33342. Dashed lines represent the Sox9+ cell population identified as tip cells. **E-H**: Kidney *Adamts18*+/+ (E, G) and *Adamts18*−/− (F, H) cryosections immunostained with Ret, EdU, and Hoechst 33342. G and H are higher magnifications of white boxes in E and F, respectively. **I**: Percentage of EdU cells in the tip populations of lungs (portion of Sox9+ population represented by dashed line showcased in B-D) and kidneys (Ret + population) in *Adamts18*+/+ and *Adamts18*−/− (n = 5). There is no significant difference in percent of EdU + cells within the tip populations of lungs or kidneys. Error bars are SD and significance was determined by a two-tailed *t*-test. All organs collected and quantified had somite counts of 51 or 52. Line in A = 200 μm; Line in B–H = 20 μm.

Within the kidney, ureteric epithelial tip cells were identified through Ret immunostaining. Again, the percentage of labelled epithelial tip cells was similar between the two genotypes: 61% in wildtype and 62% in *Adamts18*−/− kidneys (Fig. 9E–I). A similar outcome resulted with a 30 min EdU pulse, where there was little difference between the percentage of proliferating cells in lungs (70% in wildtype and 72% in *Adamts18*−/−) and kidneys (58% in wildtype and 61% in *Adamts18*−/−). Further, there was no significant Caspase 3 activity within either the lung or kidney epithelial tip populations in wildtype or *Adamts18*−/− embryos.

2.7. Expression of selected components of developmental signaling pathways reveal No difference between Adamts18−/− and wildtype tissues

To ascertain any mechanistic insights for Adamts18, we analyzed the expression of key components of important developmental signaling pathways in wildtype and Adamts18 knockout E12.5 embryos (Fig. 10A–I). We focused on four genes: *Bmp4*, *Fgf10*, *Shh*, and *Spry2*. Quantitative RNAscope analysis of the average number of transcripts per cell for each gene within the tip, stalk, and neighboring cell populations was assessed within both organs in triplicates (three tip regions analyzed per triplicate) (Fig. 10I). The expression patterns for all four genes observed in the wildtype organ systems were as expected compared to previous expression analyses (Bellusci et al., 1997; Weaver et al., 2000; Miyazaki et al., 2000; Yu et al., 2002; Pepicelli et al., 1998; Tefft et al., 1999; Hashimoto et al., 2012; Chuang et al., 2003). There was no significant difference identified between any of the genes examined, suggesting that their transcription is not affected by the lack of Adamts18 present compared to wildtype tissues.

3. Discussion

3.1. Loss of Adamts18 leads to distinct phenotypes in developing lung and kidney

In this study, we identified two distinct phenotypes within the lung and kidney in the absence of Adamts18. Whereas in the lung there is a primary requirement for Adamts18 to promote normal growth of the airways and differentiation of specialized cell types, in the kidney Adamts18 limits additional outgrowths that form a secondary collecting system. Both organs have conserved signaling programs that operate similarly to promote branching; for example, Fgf10 promotes branching through Fgfr2 (Min et al., 1998; Sekine et al., 1999; De Moerlooze et al., 2000; Ohuchi et al., 2000; Zhao et al., 2004). However, several additional RTK pathways play a role in ureteric epithelial branching, most notably the Gdnf/Ret network (Schuchardt et al., 1994; Pichel et al., 1996; Sánchez et al., 1996). Interestingly, while the evidence suggests a highly coordinated genetically hard-wired pattern of asymmetric lung bud outgrowth and branching linked to left-right asymmetry generating mechanisms (Metzger et al., 2008; Lin et al., 1999), mutational studies in the mouse and the prevalence of double ureter formation in the human population suggest a more plastic regulatory control on the initiating event in kidney organogenesis, outgrowth of the ureteric bud.

3.2. Adamts18 in the kidney

Several pathways have been identified that restrict ureteric outgrowth to a single budding event with additional branching suppressed until bud contact with the metanephric mesenchyme. Slit2 signaling through its receptor Robo2 controls axon and cell migration (Kidd et al., 1998; Kidd et al., 1999). The absence of either factor results in a highly penetrant phenotype: multiple, ectopic ureteric bud outgrowths, anterior to the normal position of outgrowth, likely a result of a loss of Slit2/Robo2 inhibition of GDNF expression in this region (Grieshammer et al., 2004; Wainwright et al., 2015). In *Adamts18*−/− embryos, the duplex ureter phenotype is weakly penetrant, and only a single ectopic outgrowth is observed.

Loss of Wnt5a or Bmp4 leads to a variety of phenotypes within the developing kidney, including double ureters. *Wnt5a* knockout mice can develop double ureters, bilateral or unilateral agenesis, hypoplasia, and duplex kidneys (Pietilä et al., 2016). However, these mutants also have post outgrowth epithelial phenotypes such as fewer branch tips and a

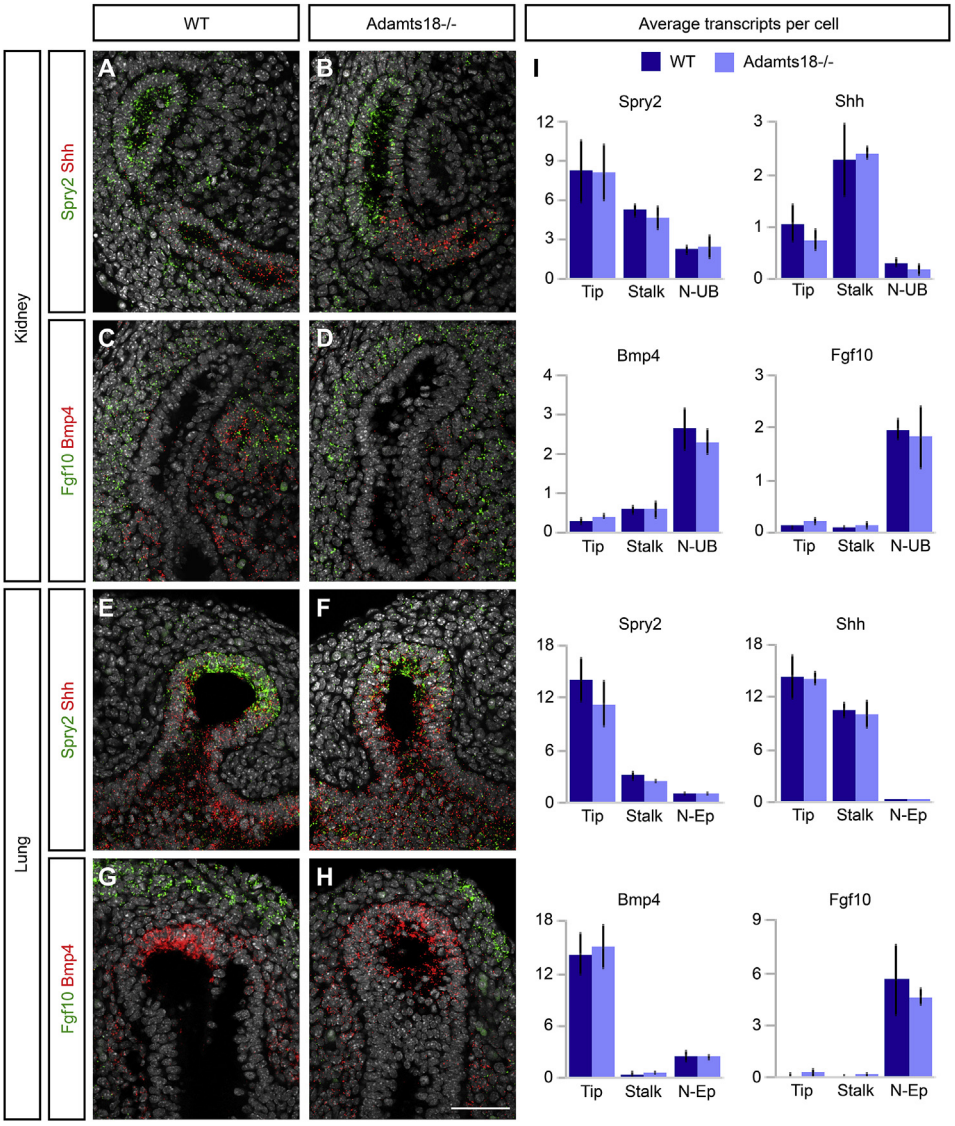

Fig. 10. Gene expression of key developmental pathway components are equivalent between *Adamts18*−/− and wildtype embryonic kidneys and lungs. A-H: Expression of *Spry2* and *Shh* (A, B, E, F) and *Fgf10* and *Bmp4* (C, D, G, H) in E12.5 kidneys (A–D) and lungs (E–H) from wildtype and *Adamts18*−/− embryos utilizing RNAscope probes. For each tissue, staining was collected from three different embryos with three images quantified from each. The number of transcripts were manually counted for three cell populations: tip, stalk, and non-ureteric bud (kidneys) or non-epithelial (lungs). **I**: The average transcripts per cell was quantified for each probe; in all cases there was no (*continued on next page*) significant difference between wildtype and *Adamts18*−/− tissue samples. Error bars are SD and significance was determined by a two-tailed *t*-test. N-UB = non-ureteric bud; N-Ep = non-epithelial. Line = 500 μm.

thickened basement membrane. Embryos heterozygous for a null mutation in *Bmp4* also display double ureters together with later phenotypes of the collecting system such as hypodysplasia, hydronephrosis, or hydroureters with high penetrance (Miyazaki et al., 2000). The double ureter phenotype associates with secondary outgrowths from the main stem of the ureteric trunk which is surrounded by strong *Bmp4* expression, suggesting a distinct origin to the ectopic branch observed in *Adamts18* mutants. In summary, the Adamts18 phenotype is quite distinct from other mutants exhibiting multiple ureteric outgrowths. It is likely that Adamts18's proteolytic activity is playing a non-essential role in turnover or modulation of some factor(s) restricting or promoting outgrowth. However, the weak penetrance of the mutant phenotype and brief period over which Adamts18 operates to regulate kidney branching makes establishing causal mechanistic links particularly difficult. Rather surprisingly given overlap in their expression, removal of Adamts16 does not enhance the Adamts18 phenotype suggesting no additional role for Adamts16 in the regulation of kidney branching. However, the deletion of the normal initiation codon in the Adamts16 alleles leaves open a possibility of abnormal translation initiation of a truncated protein at a downstream in-frame ATG. The absence of validated anti-Adamts16 antibodies precludes ruling out this caveat to the *Adamts16* mutation analysis.

In humans, double ureters have been observed in a percentage of patients with Congenital Anomaly of Kidney and Urinary Tract (CAKUT). CAKUT includes a broad spectrum of abnormalities in the development of kidney and urinary tract. Patients can have a number of anomalies, including renal agenesis, multicystic dysplastic kidneys, double ureters, congenital megaureter, and vesicoureteral reflux. CAKUT occurs in about 1 in every 500 live births and accounts for 20–30% of all congenital abnormalities (Song and Yosypiv, 2011; Uy and Reidy, 2016). Many mutated genes have been identified in CAKUT patients, some of which are conserved in mice and have been shown to play a role in the development of kidneys, such as RET, SIX2, and BMP4 (Hildebrandt, 2010; Nicolaou et al., 2015). To date, ADAMTS18 has not been identified in any CAKUT patients which may be expected from the low penetrance observed in this study but if studies were powered sufficiently, ADAMTS18-dependent ureter duplications should be a new target of interest.

3.3. *Adamts18 in the lung*

Branching of the developing mouse airways has been well-characterized: branching is genetically hard-wired with distinct modes of branching generating then expanding the five uniquely shaped lobes of the mouse lungs (Metzger et al., 2008). Interestingly, the primary phenotype observed in *Adamts18* mutant lungs at E12.5 is reduced

growth and a delay in the differentiation of specialized cell types but not in branching per se. Early branches occurred on cue, scaling to the shortened length of the primary airways. Growth retardation will eventually result in overt branching defects if there is insufficient template for branching to occur, and consistent with this view, branching defects were more readily apparent after E12.5 days in *Adamts18* mutants. Interestingly, though differentiation occurs in the lung in a proximal to distal progression and all markers examined here are thought to be present in differentiating epithelial cell types in the wild type lung by E14.5, none of these were detected at E16.5 in Adamts18 mutants. Thus, both growth and patterning are markedly disrupted by Adamts18 removal suggesting Adamts18's proteolytic activity plays a key role in coordinating these activities.

We attempted to determine whether the lung growth phenotype could be explained by a decreased proliferative activity or enhanced apoptosis in the absence of Adamts18. However, there was no apparent change in EDU incorporation in branch tips and cell death in any population. Thus, it is unlikely Adamts18 plays a role in cell survival, though it is difficult to exclude a subtle role in the proliferation of a subset of mitotically active cells in outgrowing lung epithelial or supporting mesenchyme. Interestingly, we observed a significant enhancement of growth in heterozygous *Adamts18* mutant lungs highlighting a complex association of Adamts18 levels with the lung growth phenotype. Growth and branching control have been linked to the actions of Shh, Bmp4, Fgf10, and Spry2 (Bellusci et al., 1997; Pepicelli et al., 1998; Park et al., 1998; Weaver et al., 2000; Tefft et al., 2002). However, expression studies failed to observe any change in these factors at the transcript level. This does not rule out a possible role for a secreted Adamts18 proteolytic activity in modifying the activity or distribution of these proteins directly, or through secondary modification of their interaction with Adamts18-targeted matrix proteins. Further work would be required to identify direct protein substrates of Adamts18 presumed proteolytic action.

3.4. ADAMTS18 has been implicated in a wide range of pathologies and disorders

Beyond the work here, and published studies of Adamts18's role in lens development (Ataca et al., 2016), there are a number of studies supporting roles for Adamts18 outside of organogenesis. Non-developmental studies have suggested possible actions of Adamts18 though none of these studies shed light on its substrates. ADAMTS18 has been proposed to act as a tumor suppressor since it is deleted or down-regulated in a variety of tumors, including esophageal carcinoma, nasopharyngeal carcinoma, and breast cancer (Jin et al., 2007; Xu et al., 2017). Ectopic expression of *ADAMTS18* in carcinoma cells can inhibit tumor cell growth (Jin et al., 2007). Furthermore, the methylation of *ADAMTS1*8 has been shown to be higher in cancerous tissues. Methylation dependent transcriptional silencing of *ADAMTS18* may play a broad role in cancer growth (Li et al., 2010) and additionally, mutations within *ADAMTS18* are observed in melanoma (Wei et al., 2010).

*ADAMTS1*8 has emerged as a candidate gene associated with bone mineral density, a prominent osteoporosis risk factor, in various populations (Koller et al., 2010; Xiong et al., 2009) and kyphosis, a back-curvature defect in pigs (Lindholm-Perry et al., 2010). Exome sequencing has identified *ADAMTS18* mutations in early onset severe retinal dystrophy and Knobloch syndrome, an autosomal recessive developmental disorder of the eye and the occipital region of the skull (Aldahmesh et al., 2011; Peluso et al., 2013). In contrast, in normal blood actions, thrombin enhances the secretion of ADAMTS18 and cleaves the protein, releasing a 45kD C-terminal moiety that is reported to bind and destroy platelets by oxidative platelet fragmentation (Dang et al., 2011; Li et al., 2009).

In summary, we have extended early studies of *Adamts18* mutants (Ataca et al., 2016), to demonstrate developmental roles for Adamts18 in key morphogenetic events in the kidney and lung. Future research identifying targets of Adamts18 action in the developing lung where the phenotypes are robust and penetrant will likely be the most fruitful path to an understanding of the developmental actions of Adamts18, and potential a unifying molecular link to the diverse biological actions of Adamts18 beyond mammalian organogenesis.

4. Materials and methods

4.1. Mouse strains

The *Adamts18*−/− mouse (VG 12442) was generated by the trans-NIH Knock-Out Mouse Project (KOMP) and obtained from the KOMP Repository (www.komp.org). *Adamts16* was deleted from these mice through CRISPR/Cas9 technology to generate *Adamts16*−/−;*Adamts18*−/−. The deletion was confirmed by Sanger sequencing. Mouse handling, husbandry, and procedures were all completed in compliance with the guidelines created by the Institutional Animal Care and Use Committees (IACUC) at the University of Southern California.

4.2. In situ hybridization

In situ hybridization was performed based on our previously reported procedure (Yu et al., 2012). Briefly for whole-mount *in situ* hybridization (WISH), tissue was harvested and fixed overnight in 4% paraformaldehyde (PFA), dehydrated in a methanol series, and stored in methanol at −20 °C. Samples were rehydrated and bleached with 6% hydrogen peroxide, incubated in 10 μg/ml proteinase K, fixed in 4% PFA, and pre-hybridized in hybridization buffer for 2 h followed by hybridization with RNA probes at 70 °C. Samples were transferred to a BioLane HTI machine for formamide washes, antibody incubation, and MBST [100 mM maleic acid, 150 mM NaCl, 0.1% Tween-20 (pH 7.5)] washes. To detect *in situ* hybridization, samples were incubated with BM Purple for up to 48 h, post-fixed in 4% PFA, and transferred to 80% glycerol/PBS. Tissue was imaged on an AxioZoom.V16 stereozoom microscope (Zeiss).

For section *in situ* hybridization (SISH), tissue was harvested and briefly fixed in 4% PFA, and placed in 30% sucrose overnight at 4 °C. Samples were embedded in OCT and sectioned at 12 μm (Zeiss Microm HM550 cryostat). Slides were fixed in 4% PFA overnight at 4 °C, treated with proteinase K, followed by a 4% PFA fixation. To reduce background staining, tissues were incubated in an acetylation solution (1 M triethanolamine, 0.65% HCl and 0.375% acetic anhydride) and dehydrated in 95% ethanol. Slides were hybridized overnight with RNA probes at 70 °C, then washed with 50% formamide, TNE [10 mM Tris (pH 7.5), 500 mM NaCl, 1 mM EDTA], 2 × SSC, 0.2 × SSC and MBST [100 mM maleic acid, 150 mM NaCl, 0.1 × Tween-20 (pH 7.5)] solutions. Slides were incubated with blocking solution [2% blocking reagent (Roche), 20% heat-inactivated sheep serum] for 1 h, then overnight in antibody solution at 4 °C. Samples were stained with BM Purple for up to 14 days, fixed in 4% PFA, and mounted with Glycergel (Dako). Slides were imaged on an AxioScan.Z1 (Zeiss).

RNAscope 2.5 Duplex Detection Kit and Multiplex Fluorescent v2 Kit (Advanced Cell Diagnostics) were utilized as an alternative method to the standard ISH protocols described above. Cryosections were consecutively incubated in hydrogen peroxide and protease from each kit following manufacturers' protocol. Then tissue was hybridized with RNAscope's probes at 40 °C in the HybEZ oven (Advanced Cell Diagnostics). Probe amplification and labeling occurred following manufacturer's procedure and mounted with VectaMount (Vector Laboratories) or ProLong Gold Antifade Mountant (Thermo Fisher Scientific). Tissues were imaged on an AxioScan.Z1 (Zeiss) and a confocal SP-8X (Leica). Quantification of images was done by manually counting the individual dots (each dot is a single transcript). To calculate the average number of transcripts per cell of a gene, the total number of dots was divided by the total number of cells within a cell type.

4.3. Whole-mount immunostaining

Kidneys and lungs from embryonic mice were dissected and treated to a short fixation in 4% PFA. The tissue was incubated in blocking solution (10% sheep serum, 0.1% Triton, PBS) for 1 h and then incubated in primary antibodies for 24–48 h at 4 °C. Antibodies used were pan cytokeratin (Sigma C2562, 1:500), Six2 (Proteintech 11562-1-AP, 1:500), Ret (Cell Signaling Technology 3223), vimentin (Abcam ab92547, 1:500), Sox9 (Abcam ab185230, 1:500), and Sox2 (Abcam ab97959, 1:500). The samples were rinsed in PBST (0.1%Triton, PBS) for several hours, and then incubated in the corresponding secondary antibodies for 24–48 h at 4 °C. Once the secondary antibodies were removed, the samples were washed in PBST for several hours. Tissue was imaged on an AxioZoom.V16 stereozoom microscope (Zeiss).

4.4. Three-Dimensional Tissue Analysis (Optical Projection Tomography, Tree Surveyor)

Optical Projection Tomography (OPT) and Tree Surveyor analysis were performed as per our previously published methods (Combes et al., 2014). Briefly, whole-mount fluorescently immunostained tissue was embedded in 1% low-melting point agarose, dehydrated in methanol, and cleared in BABB (1:2 benzyl alcohol, benzyl benzoate). Optically cleared samples were imaged using a custom OPT instrument. Projections were reconstructed with NRecon (Bruker microCT) to generate axial slices through the tissue. Tree Surveyor was used to analyze the branching epithelial network it identified within the slices, generating data for detailed spatial analysis (Short et al., 2013). Dendrograms were generated using Tree Surveyor data with Jstree (http://lh3lh3.users.sourceforge.net/jstree.shtml; open source program developed by Heng Li from David Reich's Lab).

4.5. Nephron counting

The protocol was adapted from the Bertram laboratory (Cullen-McEwen et al., 2012). Briefly, adult mice were perfused with cold PBS through the left ventricle of the heart to remove blood. Left kidneys were fixed with 4% PFA overnight, embedded in paraffin wax, and sectioned at 5 nm. Every 100th section and the two subsequent sections were incubated in neuraminidase at 37 °C for 30 min. Then, the sections were incubated with blocking solution (1.5% BSA, 0.1%Triton-X, PBS) for 30 min at room temperature. Peanut agglutinin (PNA, Sigma L7381) was added directly to the block solution on the tissue and incubated at 4 °C overnight. Hoechst 33342 was briefly applied to the tissue to stain nuclei. Slides were mounted with a coverslip and stored at 4 °C. Tissue was imaged with the AxioScan.Z1 (Zeiss). The first and third section of every 100th section taken throughout the entire kidney was overlaid in Photoshop. Glomeruli that were only located on only one of the two sections were counted. The total nephron count for a kidney was estimated by multiplying the total glomeruli counted by 25.

4.6. LacZ staining

Embryonic tissue was dissected and briefly fixed in 4% PFA. Whole-mount samples were permeabilized in 0.02% NP-40 and incubated at 37 °C for several hours in LacZ stain solution (5 mM $K_3Fe(CN)_6$, 5 mM $K_4Fe(CN)_6$, 2 mM $MgCl_2$, 0.01% Na deoxycholate, 0.02% NP-40, 1 mg/ml X-gal). Tissue was post-fixed in 4% PFA overnight at 4 °C and stored in 80% glycerol/PBS. Images were taken on AxioZoom.V16 stereozoom microscope (Zeiss).

Tissues for sectioning were dissected, fixed briefly with 4% PFA, incubated in 30% sucrose overnight, and embedded in OCT. Cryoblocks were sectioned at 12 µm (Zeiss Microm HM550 cryostat). Tissue was washed with 0.02% NP-40 to permeabilize, and then incubated in LacZ stain solution overnight. Fast red was used to counterstain the tissue. Slides were rinsed in water, dehydrated with ethanol, and washed in xylene. Tissue was mounted with Permount and coverslipped. Images were taken on the AxioScan.Z1 (Zeiss).

4.7. Cryosection iimmunostaining, EdU staining, and analysis

Lungs and kidneys were harvested, fixed briefly in 4% PFA, and stored overnight in 30% sucrose at 4 °C. Tissue was embedded in OCT and sectioned at 12 µm (Zeiss Microm HM550 cryostat). After 1 h incubation with block (2% sea block, 0.1% Triton-X, PBS), primary antibody was applied overnight at 4 °C. Primary antibodies used were Sox9 (Abcam ab185230, 1:1000), Ret (Cell Signaling 3223, 1:100), Caspase 3 (Novus Biologicals NB500-210, 1:1000), Prosurfactant Protein C (Millipore AB3786, 1:1000), MUC5AC (Novus Biologicals NBP2-15196, 1:1000), Acetyl-alpha tubulin (Millipore MABT868, 1:500), and E-cadherin (BD Biosciences 610181). Tissue was incubated in secondary antibody for 1 h at room temperature. After a brief incubation with Hoechst 33342, slides were imaged with the confocal SP-8X (Leica). imaged with the AxioScan.Z1 (Zeiss).

To perform EdU staining and analysis, the Click-iT EdU Alexa Fluor 647 imaging kit (Thermo Fisher C10340) was utilized following the manufacturer's protocol. Briefly, pregnant mice were injected with EdU diluted in PBS (0.04 mg EdU/gram weight of mouse) 4 h prior to collection of tissue. Cryosections were prepared and stained as described above. Additionally, EdU reaction solution (provided in the Click-iT kit) was applied to tissue for 30min. Cells were counted manually for expression of EdU, Caspase 3, Ret, and Sox9.

4.8. Quantitative polymerase chain reaction (qPCR)

RNA was isolated from dissected organs with a RNeasy Micro Kit (Qiagen 74004), and the concentration of the product was measured on the Nanodrop 2000c (Thermo Fisher). The SuperScript IV VILO kit (Thermo Fisher 1176050) was used to generate cDNA from the isolated RNA. Diluted cDNA (1:10) was added to the LUNA Universal qPCR Master Mix (New England BioLabs M3003) with primers for genes of interest in a 96-well fast plate. The plate was run on ViiA7 Real-Time PCR System (Applied Biosystems). The qPCR results were calculated through delta-delta CT analysis.

4.9. Key Resources Table

The authors have provided a Key Resources Table listing information on the resources used in this paper.

Reagent or resource	Source	Identifier
Antibodies		
Ckytokeratin (pan)	Sigma	C2562
Six2	Proteintech	11562-1-AP
Vimentin	Abcam	ab92547
Ret	Cell Signaling Technology	3223
Peanut agglutinin	Sigma	L7381
MUC5AC	Novus Biological	NBP2-15196
Prosurfactant Protein C	Millipore	AB3786
Acetyl-alpha tubulin	Millipore	MABT868
Sox9	Abcam	ab185230
Sox2	Abcam	ab97959
E-cadherin	BD Biosciences	610181
Caspase 3	Novus Biologicals	NBP2-15196
Bacterial and Virus Strains		
Biological Samples		
Chemicals, Peptides, and Recombinant Proteins		
Critical Commercial Assays		
RNAscope 2.5 Duplex Detection Kit	Advanced Cell Diagnostics	322430

(continued on next page)

(*continued*)

Reagent or resource	Source	Identifier
RNAscope Multiplex Fluorescent v2 Kit	Advanced Cell Diagnostics	323110
Click-iT EdU Alexa Fluor 647 imaging kit	Thermo Fisher	C10340
RNeasy Micro Kit	Qiagen	74004
SuperScript IV VILO kit	Thermo Fisher	1176050
Deposited Data		
Experimental Models: Cell Lines		
Experimental Models: Organisms/Strains		
Mouse: Swiss Webster	Charles River	024
Mouse: Adamts18−/−	Knock-Out Mouse Project	VG 12442
Mouse: Adamts16−/−	This paper	N/A
Oligonucleotides		
Adamts18 *in situ* probe primers: Forward: acccttgtcctgagaatagcttg Reverse: TAATACGACTCACTATAGGG gaggaattgacttgggtgtgttg	This paper	N/A
Adamts16 *in situ* probe primers: Forward: caagtggcagtttggagagaaag Reverse: TAATACGACTCACTATAGGG tagtactggttggtggaatggtg	This paper	N/A
Muc5ac qPCR primers: Forward: CAGGACTCTCTGAAATCGTACCA Reverse: AAGGCTCGTACCACAGGGA	This paper	N/A
Sftpc qPCR primers: Forward: ATGGACATGAGTAGCAAAGAGGT Reverse: CACGATGAGAAGGCGTTTGAG	This paper	N/A
Tuba4a qPCR primers: Forward: GAGATCCGAAATGGCCCATAC Reverse: GTGGAATACTAGGAAGCCCTGA	This paper	N/A
Adamts18 (Exon 3–4) qPCR primers: Forward: CCGCAGTGTTTGTATCAGGG Reverse: TACAGGACGTGAGGATGGTG	This paper	N/A
Adamts18 (Exon 10–11) qPCR primers: Forward: GGACAGATTTATGATGCCGACA Reverse: GGTGGCACCAGAGTGACTT	This paper	N/A
Adamts16 (Exon 1–2) qPCR primers: Forward: CTGAGTCCTGTGAGCCCTC Reverse: CACCGGTTTCCAGCCAGC	This paper	N/A
Adamts16 (Exon 17–18) qPCR primers: Forward: ccaaggtcaggggctaagaa Reverse: tcccgcctttgagttcatct	This paper	N/A
Gapdh qPCR primers: Forward: AGGTCGGTGTGAACGGATTTG Reverse: TGTAGACCATGTAGTTGAGGTCA	This paper	N/A
Recombinant DNA		
Software and Algorithms		
Tree Surveyor	Short et al. (2013)	N/A
NRecon	Bruker microCT	www.bruker.com
Jstree	Heng Li	http://lh3lh3.users.sourceforge.net/jstree.shtml
Other		
Adamts18 RNAscope probe	Advanced Cell Diagnostics	452251
Spry2 RNAscope probe	Advanced Cell Diagnostics	425061
Shh RNAscope probe	Advanced Cell Diagnostics	314361-C2
Bmp4 RNAscope probe	Advanced Cell Diagnostics	401301-C2
Fgf10 RNAscope probe	Advanced Cell Diagnostics	446371

Declarations of interest

None.

Funding

Work in A.P.M.'s laboratory was supported by a grant from the National Institutes of Health [DK054364]. E.A.R. was funded by a graduate student training fellowship from the National Institutes of Health [5T32HD060549] and by the National Institute of Diabetes and Digestive and Kidney Diseases of the National Institutes of Health [F31DK107216]. The funding sources were not involved in the study design, collection and analysis of data, writing the report, or the decision to submit for publication.

Acknowledgements

We thank Seth Ruffins for constructing the optical projection tomography (OPT) machine, creating the associated software, and assisting with technical troubleshooting for imaging and processing samples. We thank Gohar Saribekyan for paraffin sectioning kidneys. Additionally, we thank Young Jin Lee and Odysse Michos for their assistance with experiments.

Appendix A. Supplementary data

Supplementary data to this article can be found online at https://doi.org/10.1016/j.ydbio.2019.06.012.

References

Abdul-Majeed, S., Mell, B., Nauli, S.M., Joe, B., 2014. Cryptorchidism and infertility in rats with targeted disruption of the Adamts16 locus. PLoS One 9, e100967.

Aldahmesh, M.A., Khan, A.O., Mohamed, J.Y., Alkuraya, H., Ahmed, H., Bobis, S., Al-Mesfer, S., Alkuraya, F.S., 2011. Identification of ADAMTS18 as a gene mutated in Knobloch syndrome. J. Med. Genet. 48, 597–601.

Ataca, D., Caikovski, M., Piersigilli, A., Moulin, A., Benarafa, C., Earp, S.E., Guri, Y., Kostic, C., Arsenijevic, Y., Soininen, R., Apte, S.S., Brisken, C., 2016. Adamts18 deletion results in distinct developmental defects and provides a model for congenital disorders of lens, lung, and female reproductive tract development. Biol. Open 5, 1585–1594.

Bellusci, S., Furuta, Y., Rush, M.G., Henderson, R., Winnier, G., Hogan, B.L., 1997. Involvement of Sonic hedgehog (Shh) in mouse embryonic lung growth and morphogenesis. Development 124, 53–63.

Chi, X., Michos, O., Shakya, R., Riccio, P., Enomoto, H., Licht, J.D., Asai, N., Takahashi, M., Ohgami, N., Kato, M., Mendelsohn, C., Costantini, F., 2009. Ret-dependent cell rearrangements in the Wolffian duct epithelium initiate ureteric bud morphogenesis. Dev. Cell 17, 199–209.

Chuang, P.T., Kawcak, T., McMahon, A.P., 2003. Feedback control of mammalian Hedgehog signaling by the Hedgehog-binding protein, Hip1, modulates Fgf signaling during branching morphogenesis of the lung. Genes Dev. 17, 342–347.

Combes, A.N., Short, K.M., Lefevre, J., Hamilton, N.A., Little, M.H., Smyth, I.M., 2014. An integrated pipeline for the multidimensional analysis of branching morphogenesis. Nat. Protoc. 9, 2859–2879.

Costantini, F., Kopan, R., 2010. Patterning a complex organ: branching morphogenesis and nephron segmentation in kidney development. Dev. Cell 18, 698–712.

Cullen-McEwen, L.A., Douglas-Denton, R.N., Bertram, J.F., 2012. Estimating total nephron number in the adult kidney using the physical disector/fractionator combination. Methods Mol. Biol. 886, 333–350.

Dang, S., Bu, D., Hong, T., Zhang, W., 2011. A polyclonal antibody against active C-terminal ADAMTS-18 fragment. Hybridoma (Larchmt) 30, 567–569.

De Moerlooze, L., Spencer-Dene, B., Revest, J.M., Hajihosseini, M., Rosewell, I., Dickson, C., 2000. An important role for the IIIb isoform of fibroblast growth factor receptor 2 (FGFR2) in mesenchymal-epithelial signalling during mouse organogenesis. Development 127, 483–492.

Gopalakrishnan, K., Kumarasamy, S., Abdul-Majeed, S., Kalinoski, A.L., Morgan, E.E., Gohara, A.F., Nauli, S.M., Filipiak, W.E., Saunders, T.L., Joe, B., 2012. Targeted disruption of Adamts16 gene in a rat genetic model of hypertension. Proc. Natl. Acad. Sci. U. S. A. 109, 20555–20559.

Grieshammer, U., Le, M., Plump, A.S., Wang, F., Tessier-Lavigne, M., Martin, G.R., 2004. SLIT2-mediated ROBO2 signaling restricts kidney induction to a single site. Dev. Cell 6, 709–717.

Hashimoto, S., Nakano, H., Suguta, Y., Singh, G., Katyal, S.L., 2012. Immunolocalization of sprouty-1 and sprouty-2 in developing rat lung. Pathobiology 79, 34–44.

Hildebrandt, F., 2010. Genetic kidney diseases. Lancet 375, 1287–1295.

Iber, D., Menshykau, D., 2013. The control of branching morphogenesis. In: Open Biol, vol 3, p. 130088 (England).

Jin, H., Wang, X., Ying, J., Wong, A.H., Li, H., Lee, K.Y., Srivastava, G., Chan, A.T., Yeo, W., Ma, B.B., Putti, T.C., Lung, M.L., Shen, Z.Y., Xu, L.Y., Langford, C., Tao, Q., 2007. Epigenetic identification of ADAMTS18 as a novel 16q23.1 tumor suppressor frequently silenced in esophageal, nasopharyngeal and multiple other carcinomas. Oncogene 26, 7490–7498.

Kelwick, R., Desanlis, I., Wheeler, G.N., Edwards, D.R., 2015. The ADAMTS (A disintegrin and metalloproteinase with thrombospondin motifs) family. Genome Biol. 16, 113.
Kidd, T., Bland, K.S., Goodman, C.S., 1999. Slit is the midline repellent for the robo receptor in Drosophila. Cell 96, 785–794.
Kidd, T., Brose, K., Mitchell, K.J., Fetter, R.D., Tessier-Lavigne, M., Goodman, C.S., Tear, G., 1998. Roundabout controls axon crossing of the CNS midline and defines a novel subfamily of evolutionarily conserved guidance receptors. Cell 92, 205–215.
Koller, D.L., Ichikawa, S., Lai, D., Padgett, L.R., Doheny, K.F., Pugh, E., Paschall, J., Hui, S.L., Edenberg, H.J., Xuei, X., Peacock, M., Econs, M.J., Foroud, T., 2010. Genome-wide association study of bone mineral density in premenopausal European-American women and replication in African-American women. J. Clin. Endocrinol. Metab. 95, 1802–1809.
Kumar, S., Rao, N., Ge, R., 2012. Emerging roles of ADAMTSs in angiogenesis and cancer. Cancers (Basel) 4, 1252–1299.
Kuure, S., Chi, X., Lu, B., Costantini, F., 2010. The transcription factors Etv4 and Etv5 mediate formation of the ureteric bud tip domain during kidney development. Development 137, 1975–1979.
Li, Z., Nardi, M.A., Li, Y.S., Zhang, W., Pan, R., Dang, S., Yee, H., Quartermain, D., Jonas, S., Karpatkin, S., 2009. C-terminal ADAMTS-18 fragment induces oxidative platelet fragmentation, dissolves platelet aggregates, and protects against carotid artery occlusion and cerebral stroke. Blood 113, 6051–6060.
Li, Z., Zhang, W., Shao, Y., Zhang, C., Wu, Q., Yang, H., Wan, X., Zhang, J., Guan, M., Wan, J., Yu, B., 2010. High-resolution melting analysis of ADAMTS18 methylation levels in gastric, colorectal and pancreatic cancers. Med. Oncol. 27, 998–1004.
Lin, C.R., Kioussi, C., O'Connell, S., Briata, P., Szeto, D., Liu, F., Izpisua-Belmonte, J.C., Rosenfeld, M.G., 1999. Pitx2 regulates lung asymmetry, cardiac positioning and pituitary and tooth morphogenesis. Nature 401, 279–282.
Lindholm-Perry, A.K., Rohrer, G.A., Kuehn, L.A., Keele, J.W., Holl, J.W., Shackelford, S.D., Wheeler, T.L., Nonneman, D.J., 2010. Genomic regions associated with kyphosis in swine. BMC Genet. 11, 112.
McMahon, A.P., 2016. Development of the mammalian kidney. Curr. Top. Dev. Biol. 117, 31–64.
Metzger, R.J., Klein, O.D., Martin, G.R., Krasnow, M.A., 2008. The branching programme of mouse lung development. Nature 453, 745–750 (England).
Michael, L., Davies, J.A., 2004. Pattern and regulation of cell proliferation during murine ureteric bud development. J. Anat. 204, 241–255.
Min, H., Danilenko, D.M., Scully, S.A., Bolon, B., Ring, B.D., Tarpley, J.E., DeRose, M., Simonet, W.S., 1998. Fgf-10 is required for both limb and lung development and exhibits striking functional similarity to Drosophila branchless. Genes Dev. 12, 3156–3161.
Miyazaki, Y., Oshima, K., Fogo, A., Hogan, B.L., Ichikawa, I., 2000. Bone morphogenetic protein 4 regulates the budding site and elongation of the mouse ureter. J. Clin. Investig. 105, 863–873.
Morrisey, E.E., Hogan, B.L., 2010. Preparing for the first breath: genetic and cellular mechanisms in lung development. Dev. Cell 18, 8–23.
Nation, E.F., 1944. Duplication of the kidney and ureter: a statistical study of 230 new cases. J. Urol. 51, 456–465.
Nicolaou, N., Renkema, K.Y., Bongers, E.M., Giles, R.H., Knoers, N.V., 2015. Genetic, environmental, and epigenetic factors involved in CAKUT. Nat. Rev. Nephrol. 11, 720–731.
Ochoa-Espinosa, A., Affolter, M., 2012. Branching morphogenesis: from cells to organs and back. Cold Spring Harb. Perspect. Biol. 4.
Ohuchi, H., Hori, Y., Yamasaki, M., Harada, H., Sekine, K., Kato, S., Itoh, N., 2000. FGF10 acts as a major ligand for FGF receptor 2 IIIb in mouse multi-organ development. Biochem. Biophys. Res. Commun. 277, 643–649.
Osathanondh, V., Potter, E.L., 1963. Development of human kidney as shown by microdissection. III. formation and interrelationship of collecting tubules and nephrons. Arch. Pathol. 76, 290–302.
Pal, A., Reidy, K.J., 2017. Genetic syndromes affecting kidney development. Results Probl. Cell Differ. 60, 257–279.
Park, W.Y., Miranda, B., Lebeche, D., Hashimoto, G., Cardoso, W.V., 1998. FGF-10 is a chemotactic factor for distal epithelial buds during lung development. Dev. Biol. 201, 125–134.
Peluso, I., Conte, I., Testa, F., Dharmalingam, G., Pizzo, M., Collin, R.W., Meola, N., Barbato, S., Mutarelli, M., Ziviello, C., Barbarulo, A.M., Nigro, V., Melone, M.A., Simonelli, F., Banfi, S., 2013. The ADAMTS18 gene is responsible for autosomal recessive early onset severe retinal dystrophy. Orphanet J. Rare Dis. 8, 16.
Pepicelli, C.V., Lewis, P.M., McMahon, A.P., 1998. Sonic hedgehog regulates branching morphogenesis in the mammalian lung. Curr. Biol. 8, 1083–1086.
Pichel, J.G., Shen, L., Sheng, H.Z., Granholm, A.C., Drago, J., Grinberg, A., Lee, E.J., Huang, S.P., Saarma, M., Hoffer, B.J., Sariola, H., Westphal, H., 1996. Defects in enteric innervation and kidney development in mice lacking GDNF. Nature 382, 73–76.
Pietila, I., Prunskaite-Hyyrylainen, R., Kaisto, S., Tika, E., van Eerde, A.M., Salo, A.M., Garma, L., Miinalainen, I., Feitz, W.F., Bongers, E.M., Juffer, A., Knoers, N.V., Renkema, K.Y., Myllyharju, J., Vainio, S.J., 2016. Wnt5a deficiency leads to anomalies in ureteric tree development, tubular epithelial cell organization and basement membrane integrity pointing to a role in kidney collecting duct patterning. PLoS One 11, e0147171.
Riccio, P., Cebrian, C., Zong, H., Hippenmeyer, S., Costantini, F., 2016. Ret and Etv4 promote directed movements of progenitor cells during renal branching morphogenesis. PLoS Biol. 14, e1002382.
Rutledge, E.A., Benazet, J.D., McMahon, A.P., 2017. Cellular heterogeneity in the ureteric progenitor niche and distinct profiles of branching morphogenesis in organ development. Development 144, 3177–3188.
Sanchez, M.P., Silos-Santiago, I., Frisen, J., He, B., Lira, S.A., Barbacid, M., 1996. Renal agenesis and the absence of enteric neurons in mice lacking GDNF. Nature 382, 70–73.
Saxen, L., Sariola, H., 1987. Early organogenesis of the kidney. Pediatr. Nephrol. 1, 385–392.
Schuchardt, A., D'Agati, V., Larsson-Blomberg, L., Costantini, F., Pachnis, V., 1994. Defects in the kidney and enteric nervous system of mice lacking the tyrosine kinase receptor Ret. Nature 367, 380–383.
Sekine, K., Ohuchi, H., Fujiwara, M., Yamasaki, M., Yoshizawa, T., Sato, T., Yagishita, N., Matsui, D., Koga, Y., Itoh, N., Kato, S., 1999. Fgf10 is essential for limb and lung formation. Nat. Genet. 21, 138–141.
Short, K., Hodson, M., Smyth, I., 2013. Spatial mapping and quantification of developmental branching morphogenesis. Development 140, 471–478.
Song, R., Yosypiv, I.V., 2011. Genetics of congenital anomalies of the kidney and urinary tract. Pediatr. Nephrol. 26, 353–364.
Stanton, H., Melrose, J., Little, C.B., Fosang, A.J., 2011. Proteoglycan degradation by the ADAMTS family of proteinases. Biochim. Biophys. Acta 1812, 1616–1629.
Tefft, J.D., Lee, M., Smith, S., Leinwand, M., Zhao, J., Bringas Jr., P., Crowe, D.L., Warburton, D., 1999. Conserved function of mSpry-2, a murine homolog of Drosophila sprouty, which negatively modulates respiratory organogenesis. Curr. Biol. 9, 219–222.
Tefft, D., Lee, M., Smith, S., Crowe, D.L., Bellusci, S., Warburton, D., 2002. mSprouty2 inhibits FGF10-activated MAP kinase by differentially binding to upstream target proteins. Am. J. Physiol. Lung Cell Mol. Physiol. 283, L700–L706.
Uy, N., Reidy, K., 2016. Developmental genetics and congenital anomalies of the kidney and urinary tract. J. Pediatr. Genet. 5, 51–60.
Wainwright, E.N., Wilhelm, D., Combes, A.N., Little, M.H., Koopman, P., 2015. ROBO2 restricts the nephrogenic field and regulates Wolffian duct-nephrogenic cord separation. Dev. Biol. 404, 88–102.
Weaver, M., Dunn, N.R., Hogan, B.L., 2000. Bmp4 and Fgf10 play opposing roles during lung bud morphogenesis. Development 127, 2695–2704.
Wei, X., Prickett, T.D., Viloria, C.G., Molinolo, A., Lin, J.C., Cardenas-Navia, I., Cruz, P., Rosenberg, S.A., Davies, M.A., Gershenwald, J.E., Lopez-Otin, C., Samuels, Y., 2010. Mutational and functional analysis reveals ADAMTS18 metalloproteinase as a novel driver in melanoma. Mol. Cancer Res. 8, 1513–1525.
Weibel, E.R., Gomez, D.M., 1962. Architecture of the human lung. Use of quantitative methods establishes fundamental relations between size and number of lung structures. Science 137, 577–585.
Xiong, D.H., Liu, X.G., Guo, Y.F., Tan, L.J., Wang, L., Sha, B.Y., Tang, Z.H., Pan, F., Yang, T.L., Chen, X.D., Lei, S.F., Yerges, L.M., Zhu, X.Z., Wheeler, V.W., Patrick, A.L., Bunker, C.H., Guo, Y., Yan, H., Pei, Y.F., Zhang, Y.P., Levy, S., Papasian, C.J., Xiao, P., Lundberg, Y.W., Recker, R.R., Liu, Y.Z., Liu, Y.J., Zmuda, J.M., Deng, H.W., 2009. Genome-wide association and follow-up replication studies identified ADAMTS18 and TGFBR3 as bone mass candidate genes in different ethnic groups. Am. J. Hum. Genet. 84, 388–398.
Xu, H., Xiao, Q., Fan, Y., Xiang, T., Li, C., Li, S., Hui, T., Zhang, L., Li, H., Li, L., Ren, G., 2017. Epigenetic silencing of ADAMTS18 promotes cell migration and invasion of breast cancer through AKT and NF-kappaB signaling. Cancer Med. 6, 1399–1408.
Yu, J., Valerius, M.T., Duah, M., Staser, K., Hansard, J.K., Guo, J.J., McMahon, J., Vaughan, J., Faria, D., Georgas, K., Rumballe, B., Ren, Q., Krautzberger, A.M., Junker, J.P., Thiagarajan, R.D., Machanick, P., Gray, P.A., van Oudenaarden, A., Rowitch, D.H., Stiles, C.D., Ma, Q., Grimmond, S.M., Bailey, T.L., Little, M.H., McMahon, A.P., 2012. Identification of molecular compartments and genetic circuitry in the developing mammalian kidney. Development 139, 1863–1873.
Zhao, H., Kegg, H., Grady, S., Truong, H.T., Robinson, M.L., Baum, M., Bates, C.M., 2004. Role of fibroblast growth factor receptors 1 and 2 in the ureteric bud. Dev. Biol. 276, 403–415.